12. C. M. Niemeyer, B. Ceyhan, *Angew. Chem. Int. Ed.* **40**, 3685 (2001).
13. O. D. Velev, E. W. Kaler, *Langmuir* **15**, 3693 (1999).
14. S.-J. Park *et al.*, *Angew. Chem. Int. Ed.* **39**, 3845 (2000).
15. R. Moller, A. Csaki, J. M. Kohler, W. Fritzsche, *Langmuir* **17**, 5426 (2001).
16. S. P. A. Fodor, *Science* **277**, 393 (1997).
17. L. A. Chrisey, G. U. Lee, C. E. O'Ferrall, *Nucleic Acids Res.* **24**, 3031 (1996).
18. F. Eckstein, *Oligonucleotides and Analogues* (Oxford Univ. Press, New York, 1991).
19. S. Ikuta, K. Takagi, R. B. Wallace, K. Itakura, *Nucleic Acids Res.* **15**, 797 (1987).
20. Supplementary data are available on *Science* Online at www.sciencemag.org/cgi/content/full/295/5559/1503/DC1.
21. The nanoparticle coverage on the ITO surface does not necessarily correspond exactly with the coverage on the SiO_2 surface. However, the SEM images provide information about the silver-deposition process on an oxide surface modified with oligonucleotide-functionalized nanoparticles rather than a correlation between the amount of deposited silver and resistance values in Fig. 2.
22. C.A.M. acknowledges the Air Force Office of Scientific Research (DURINT) and the Defense Advanced Research Projects Agency for support of this research.

10 October 2001; accepted 17 January 2002

Efficient Near-Infrared Polymer Nanocrystal Light-Emitting Diodes

Nir Tessler,[1]* Vlad Medvedev,[1] Miri Kazes,[2] ShiHai Kan,[2] Uri Banin[2]*

Conjugated polymers and indium arsenide–based nanocrystals were used to create near-infrared plastic light-emitting diodes. Emission was tunable from 1 to 1.3 micrometers—a range that effectively covers the short-wavelength telecommunications band—by means of the quantum confinement effects in the nanocrystals. The external efficiency value (photons out divided by electrons in) is ~0.5% (that is, >1% internal) and is mainly limited by device architecture. The near-infrared emission did not overlap the charge-induced absorption bands of the polymer.

For certain device applications, semiconducting polymers can replace inorganic semiconductors at lower cost because they are more easily processed. Examples include the development of organic light-emitting diodes (OLEDs) for full-color screen applications, and the development of field-effect transistors for smart circuit applications (*1, 2*). The extension of OLEDs into the technologically important near-infrared (NIR) spectral range used in telecommunications is more difficult because organic molecules usually display optical activity only at wavelengths shorter than 1 μm.

Attempts have been made to extend organic-based light emission beyond 1 μm by using lanthanide complexes in which rare-earth atoms are incorporated into the molecules (*3–5*). Emission efficiency is generally low because of near-field deactivation by the host associated with coupling of the optically excited state to the vibrations of the organic molecule or polymer (*6*), the best reported internal efficiency value being 0.01% (*7*). Furthermore, the 1.5-μm band is effectively covered by the mature technology of erbium-doped fiber amplifiers (*8*), whereas similar devices for the 1.3-μm band are still being developed. Here we report the production of OLEDs, based on a combination of semiconducting polymers and NIR optically active semiconductor nanocrystals (NCs) (*9*), that cover the short-wavelength telecommunications band with internal efficiency values of >1%.

The incorporation of NCs with a semiconducting polymer in visible-range OLEDs (*10–13*) and photovoltaics (*14*) has been reported. We used a core-shell approach to produce NCs with strong emission in the NIR and increased photostability (*15, 16*). Optimized core-shell NC structures can shield the electron-hole pair that is localized to the core from the host deactivation paths while still allowing this active region to absorb energy from the host, either through charge transfer or through neutral-excitation energy transfer (as in the case of Förster or Dexter transfer mechanisms) (*17*). In combination with commercially available polymers (*18*), we fabricated LEDs with external efficiencies up to 0.5% [corresponding to 1.5 to 3% internal efficiency (*19, 20*)] where the emission center can be tuned up to 1.3 μm and the emission tail extends beyond 1.4 μm. The emission is taken out of the charge-induced absorption bands of the polymer (centered around ~800 nm), thus overcoming what is considered to be the main obstacle for achieving electrically pumped lasers in amorphous organic materials (*21*).

Core-shell InAs-ZnSe NCs with an average core radius of 2.4 nm and ZnSe shell with nominal thickness of 1.5 monolayers (Fig. 1A) with strong emission in the 1.3-μm range were prepared in a two-step synthesis, as reported previously (*15, 16*). Films of conjugated polymers—either poly[2-methoxy-5-(2-ethylhexyloxy)-1,4-phenylenevinylene] (MEH-PPV) or poly[(9,9-dihexylfluorenyl-2,7-diyl)-co-(1,4-{benzo-[2,1′,3]thiadiazole})] (F6BT) (Fig. 1) (*18, 22*)—and NCs were made by first creating separate NC and polymer solutions in toluene. Appropriate volumes were mixed to create the required NC/polymer volume ratio. Finally, the optical absorption of the composite film was measured and used as a final monitoring step. Optically homogeneous films were spin-cast from solution to ~100 nm thickness onto a suitable substrate (*23*). Typical absorption spectra of such films are shown in Fig. 1B. The absorption is essentially a combination of the two species. Above 800 nm, the absorption is due to quantum-confined transitions of the NCs, and below 600 nm, the host conjugated polymer contributes considerably,

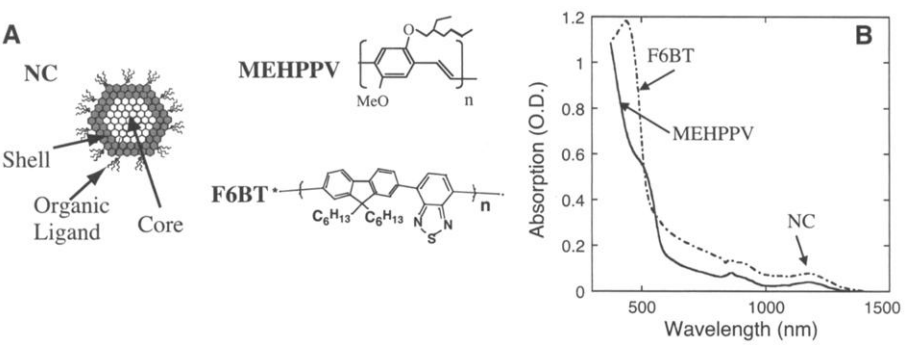

Fig. 1. (**A**) Structural description of the nanocrystal (NC) and of the polymers MEH-PPV and F6BT. (**B**) Optical absorption spectra of MEH-PPV–NC (solid line) and F6BT-NC (dashed line) films with approximately equal volume ratio.

[1]Electrical Engineering Department, Microelectronic Center, and Communications and Information Technologies Center, Technion–Israel Institute of Technology, Haifa 32000, Israel. [2]Institute of Chemistry and the Center for Nanoscience and Nanotechnology, Hebrew University, Jerusalem 91904, Israel.

*To whom correspondence should be addressed. E-mail: nir@ee.technion.ac.il, banin@chem.ch.huji.ac.il

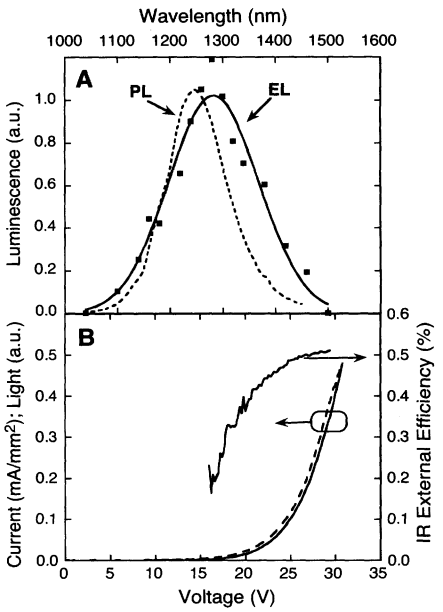

Fig. 2. (**A**) The PL spectrum of InAs-ZnSe NCs in toluene solution (dashed line) and the EL spectrum of a polymer-NC (MEH-PPV as host, squares and solid line) LED. The EL spectrum was measured, inside the glove box, with a set of 20-nm-wide bandpass filters. (**B**) Current (dashed line), light (solid line), and external efficiency (solid line, right axis) as a function of applied voltage measured for the MEH-PPV–NC LED. The maximum external efficiency reaches 0.5%.

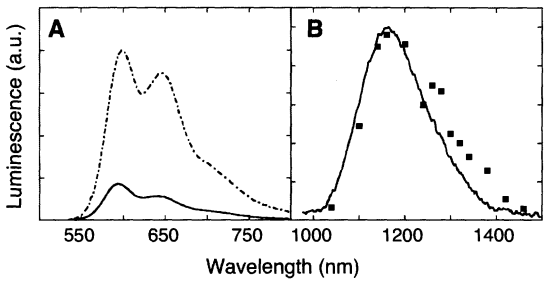

Fig. 3. (**A**) The PL for polymer-only (dot-dashed line) versus polymer-NC (solid line) films, exhibiting a reduction in the polymer emission attributed to energy transfer. (**B**) The PL (line) and EL (squares) band seen for the NCs in the combined polymer-NC film.

in addition to the contribution of the high-energy tail of the NC absorption.

Figure 2A shows the photoluminescence (PL, dashed line) and electroluminescence (EL, solid line and points) spectra of one batch of NCs. The width of the peak at 1270 nm is largely attributed to the inhomogeneous broadening caused by the size distribution of the particles. The EL spectrum for the LEDs we fabricated shows a slight red shift toward 1300 nm. Such a red shift is also present in close-packed films of InAs NCs and is attributed to energy transfer from small to large NCs.

The electrical characteristics of the LED are summarized in Fig. 2B. We estimated the external efficiency of the NIR emission by measuring the light intensity in the forward direction and converting it into total external emission by assuming the external emission profile to be Lambertian (*24*). Although the external efficiency reaches ~0.5%, the turn-on voltage is rather high (~15 V), indicating that the device structure is not optimal. The voltage dependence of the efficiency suggests (*25*) that this relatively high efficiency value is limited by imbalanced injection and transport of electrons and holes.

To better understand the device characteristics, and to demonstrate the wavelength tunability afforded by controlling the NC size, we also prepared LEDs using InAs-ZnSe core-shell structures with core radii of 2 nm and nominal shell thickness of 1.5 monolayers. For the PL measurements of MEH-PPV–NC (1:1 volume %) and polymer only, films were prepared on glass substrates by drop-casting and excited at 510 nm. Figure 3A shows a significant but noncomplete reduction (by a factor of ~5) of the visible PL intensity in the composite film. This difference provides evidence for the role of energy transfer between the polymer host and the NCs in such films. The PL of the NCs shown in Fig. 3B (solid line) is centered at 1160 nm in this case, again red-shifted compared to the solution PL (centered at 1110 nm). The EL spectrum of an LED (device 4 in Fig. 4), made using the same composite ratio, is also shown in Fig. 3B (squares), and it nearly overlaps the PL of the film. In the EL case, the visible emission was negligibly small.

The electrical and optical behavior of the LEDs was studied by changing the volume content of these NCs in the film. We prepared LEDs based on MEH-PPV in which the NC/polymer volume ratio was 0:1 (device 0), 1:8 (device 1), 1:4 (device 2), 1:2 (device 3), and 1:1 (device 4). All curves were measured up to a maximum current of 1.5 mA (sweep time <10 s). Figure 4A shows the current-voltage (*I-V*) curves for the different LEDs. The turn-on voltage for the pure MEH-PPV sample (device 0) is ~2 V and increases as the NC content increases. Figure 4B shows the corresponding dependence of the NIR light-emission intensity on voltage. The enhancement of the maximum light-emission intensity as the NC content increases directly reflects the enhanced efficiency. Device 0 exhibits a bright orange emission that is typical of MEH-PPV (no NIR emission). Device 4, however, shows a strong NIR emission with only a negligibly small visible emission. Devices 1, 2, and 3 follow the trend between devices 0 and 4. The negligibly small visible emission in device 4 indicates that a charge-transfer mechanism is playing an important role on top of the energy transfer, shown in Fig. 3. Therefore, the enhanced efficiency is also associated with electronic trapping at the NC sites. The enhanced turn-on voltage is consistent with the presence of trapping effects (*26*). The above features suggest (*25*) that although the characteristics of the LED

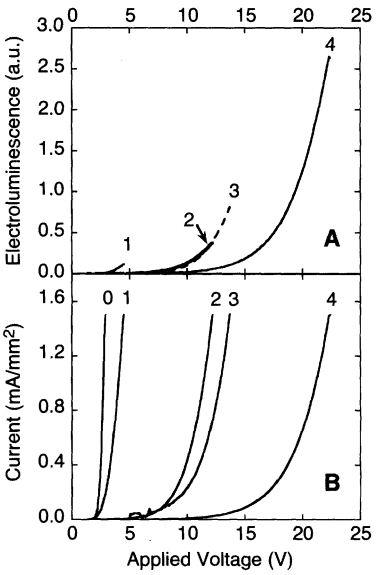

Fig. 4. (**A**) Light-voltage and (**B**) current-voltage characteristics of a set of MEH-PPV–NC LEDs. Within the set the NC/polymer volume ratio was 0:1 (device 0), 1:8 (device 1), 1:4 (device 2), 1:2 (device 3), and 1:1 (device 4). Note that as the volume ratio goes up, both the turn-on voltage and the light-emission efficiency increase. To ensure measurements of IR emission only, we placed a filter in front of the detector (OD-5 long-pass filter cutting at 1060 nm). Similar results (but with lower efficiency) were obtained with the F6BT-based composites.

structure—such as active-layer thickness and contact material—were close to optimum for pure MEH-PPV films, this was not the case for the polymer-NC device, thus requiring relatively high voltage to achieve the highest efficiency value.

The compatibility of the nanocomposite constituents can be further improved by choosing other polymers or a different core-shell design, or by adding other elements to create cascade energy transfer from the host to the NC guest. By tailoring the energy levels of the polymer and NCs, it should also be possible to produce solution-processable detectors at NIR wavelength range. Finally, by changing the NC chemical constituents with suitable control of the core and shell material and size, it should be possible to extend the emission to the 1.5-μm range and thus provide low-cost solutions for the "fiber to the home" telecommunications problem.

References and Notes

1. A. Dodabalapur *et al.*, *Appl. Phys. Lett.* **73**, 142 (1998).
2. H. Sirringhaus, N. Tessler, R. H. Friend, *Science* **280**, 1741 (1998).
3. R. J. Curry, W. P. Gillin, *Appl. Phys. Lett.* **75**, 1380 (1999).
4. L. H. Slooff *et al.*, *Appl. Phys. Lett.* **78**, 2122 (2001).
5. Y. Kawamura, Y. Wada, M. Iwamuro, T. Kitamura, S. Yanagida, *Chem. Lett.* **2000**, 280 (2000).
6. L. H. Slooff *et al.*, *J. Appl. Phys.* **83**, 497 (1998).
7. R. J. Curry, W. P. Gillin, A. P. Knights, R. Gwilliam, *Opt. Mater.* **17**, 161 (2001).
8. E. Desurvire, *Erbium Doped Fiber Amplifiers: Principles and Applications* (Wiley, New York, 1994).
9. A. D. Yoffe, *Adv. Phys.* **50**, 1 (2001).
10. V. L. Colvin, M. C. Schlamp, A. P. Alivisatos, *Nature* **370**, 354 (1994).
11. B. O. Dabbousi, M. G. Bawendi, O. Onitsuka, M. F. Rubner, *Appl. Phys. Lett.* **66**, 1316 (1995).
12. M. C. Schlamp, X. G. Peng, A. P. Alivisatos, *J. Appl. Phys.* **82**, 5837 (1997).
13. H. Mattoussi *et al.*, *J. Appl. Phys.* **83**, 7965 (1998).
14. N. C. Greenham, X. G. Peng, A. P. Alivisatos, *Phys. Rev. B* **54**, 17628 (1996).
15. Y. W. Cao, U. Banin, *Angew. Chem. Int. Ed. Engl.* **38**, 3692 (1999).
16. ———, *J. Am. Chem. Soc.* **122**, 9692 (2000).
17. M. A. Baldo, M. E. Thompson, S. R. Forrest, *Nature* **403**, 750 (2000).
18. ADSDYES, www.adsdyes.com (American Dye Source Inc.).
19. The conversion from external to internal efficiency in subwavelength devices depends on many device parameters (*20*), and hence we can only estimate a range for the internal efficiency of 1.5 to 3%.
20. N. Tessler, *Appl. Phys. Lett.* **77**, 1897 (2000).
21. ———, in *Elsevier Encyclopedia of Materials: Science and Technology*, E. J. Kramer, G. Hadziioannou, Eds. (Elsevier, New York, 2001), pp. 4402–4408.
22. The conjugated polymer hosts were used as purchased (MEH-PPV or ADS100RE and F6BT or ADS133) without any additional chemical treatment.
23. Glass or indium tin oxide (ITO)–glass substrates were used for optical and electrical measurements, respectively. The nanocomposite solution was prepared by first preparing NC and polymer solutions in toluene having weight concentrations of ~50 mg/ml and 5 mg/ml, respectively. The LED preparation procedure was as follows: The ITO-glass substrate was plasma-cleaned and then covered by PEDOT (Bayer Baytron P TP Al), which was then annealed at 110°C for 30 min. After substrate cooling, the nanocomposite solution (~1:1 volume ratio) was spin-coated on the ITO-PEDOT substrate with a resulting thickness of ~100 nm. This structure was then annealed at 90°C for 30 min and allowed to slowly cool down under dry vacuum. Finally, Ca-Al contacts were evaporated at working pressure within the low (10^{-7} mbar) range. Pixel area was 1 mm by 1 mm. All steps, including optical and electrical characterization of the LEDs, were carried out within an inert glove box system having sub-ppm levels of water and oxygen.
24. N. C. Greenham, R. H. Friend, D. D. C. Bradley, *Adv. Mater.* **6**, 491 (1994).
25. G. G. Malliaras, J. C. Scott, *J. Appl. Phys.* **83**, 5399 (1998).
26. K. C. Kao, W. Hwang, *Electrical Transport in Solids*, vol. 14 of *International Series in the Science of the Solid State* (Pergamon, New York, 1981).

27. We thank R. Beadle for his help with the experimental setup. Supported in part by Israel Science Foundation grants 99/00-12.5 (U.B.) and 56/00-11.6 (N.T.).

19 November 2001; accepted 17 January 2002

Otolith $\delta^{18}O$ Record of Mid-Holocene Sea Surface Temperatures in Peru

C. Fred T. Andrus,[1]* Douglas E. Crowe,[1] Daniel H. Sandweiss,[2] Elizabeth J. Reitz,[3] Christopher S. Romanek[1,4]

Peruvian sea catfish (*Galeichthys peruvianus*) sagittal otoliths preserve a record of modern and mid-Holocene sea surface temperatures (SSTs). Oxygen isotope profiles in otoliths excavated from Ostra [6010 ± 90 years before the present (yr B.P.); 8°55′S] indicate that summer SSTs were ~3°C warmer than those of the present. Siches otoliths (6450 ± 110 yr B.P.; 4°40′S) recorded mean annual temperatures ~3° to 4°C warmer than were measured under modern conditions. Trophic level and population diversity and equitability data from these faunal assemblages and other Peruvian archaeological sites support the isotope interpretations and suggest that upwelling of the Peru-Chile current intensified after ~5000 yr B.P.

Evidence that modern El Niño–Southern Oscillation (ENSO) conditions (e.g., Pacific SSTs, precipitation, and frequency of El Niño warm events) began after the mid-Holocene is increasing. Ecuadorian lake sediments record lower frequency ENSO before 5000 yr B.P. (*1*, *2*). Western Pacific coral oxygen isotope ($\delta^{18}O$) and Sr/Ca data document warmer western Pacific SSTs, increased evaporation ~5350 yr B.P. (*3*), and decreased ENSO ~6500 yr B.P. (*4*). Western Pacific terrestrial pollen records suggest that ENSO was less active before ~4000 yr B.P. (*5*). Ice cores from Huascarán, Peru, indicate that the local climate was warmer than the modern climate from 8400 to 5200 yr B.P. (*6*). Thermally anomalous molluscan assemblages (TAMAs) and tropical fish in Peruvian middens north of 10°S suggest that there were warmer SSTs in the eastern Pacific from ~8000 to 5000 yr B.P. (*7*, *8*). Model results for 6 and 11 thousand years ago suggest a slightly warmer annual mean SST along the coast of Ecuador and northern Peru than at present (*9*).

In contrast, some ENSO climate models incorporating seasonality changes caused by perihelion timing indicate a cool eastern Pacific before 5000 yr B.P. (*10*, *11*). Field evidence of a cool mid-Holocene eastern Pacific includes Peruvian coastal geomorphology and soils that suggest persistent aridity (*12*, *13*). Advocates of this position argue that TAMAs (*7*, *8*) resulted from restricted warm-water embayments protecting species that would otherwise not survive in the cool open ocean (*8*, *12*, *14*).

The lack of quantitative seasonal SST data from mid-Holocene northern coastal Peru makes it difficult to resolve these different interpretations (*7*, *11*). Our otolith data provide SST reconstructions that indicate that the eastern Pacific at ~6000 yr B.P. was seasonally warmer than today along the central coast of Peru and warmer year-round along the northern coast of Peru.

Otoliths are aragonite ($CaCO_3$) structures in fish used for acoustic perception and balance. They grow incrementally from the endolymph in alternating opaque and translucent bands that reflect biological and environmental growth conditions (*15*). Previous studies show that otolith aragonite precipitates in oxygen isotope equilibrium with seawater (*16*). The exchange reaction is temperature dependent; thus, the $\delta^{18}O$ composition of the otolith can be used as a temperature proxy (*16*, *17*).

The archaeological sites of Ostra (6250 ± 250 to 5160 ± 60 yr B.P.) and Siches (6590 ± 90 to 4930 ± 80 yr B.P.) are central to interpretations of warm eastern Pacific SSTs from 8000 to 5000 yr B.P. (*7*, *8*). Ostra is currently in a warm-temperate area, and Siches is transitional between the warm-tropical Panamanian and the cooler warm-temperate Peru-Chile provinces (Fig. 1). Both sites contain well-preserved otolith assemblages of several species, including *Galeichthys peruvianus* (*7*, *18*).

G. peruvianus was selected for analysis because it does not migrate, even in response to seasonal or ENSO-related SST changes. Typically, Ariidae catfish remain in nearshore habitats (*19*). They have large otoliths containing biannual growth banding, thus making them amenable to microsampling (Fig. 2). Modern *G. peruvianus* were caught

[1]Department of Geology, University of Georgia, Athens, GA 30602–2501, USA. [2]Department of Anthropology and Institute for Quaternary Research, S. Stevens Hall, University of Maine, Orono, ME 04469, USA. [3]Department of Anthropology and Georgia Museum of Natural History, Natural History Building, University of Georgia, Athens, GA 30602–1882, USA. [4]Savannah River Ecology Laboratory, Drawer E, Aiken, SC 29802, USA.

*To whom correspondence should be addressed. E-mail: andrus@gly.uga.edu